

Divertor Design Study on Compact DEMO Reactor for Handling of Huge Exhaust Power

H.Kawashima, K.Shimizu, T.Takizuka, K.Tobita, S.Nishio, S.Sakurai, H.Takenaga

Japan Atomic Energy Agency, Naka, Ibaraki-ken, 311-0193 Japan

e-mail contact of main author: kawashima.hisato@jaea.go.jp

Abstract. For the divertor design study of a compact DEMO reactor, Slim CS, using SOLDOR/NEUT2D code, we estimated a prospect of handling huge exhausted power in the divertor. Assuming the exhausted power of 500 MW and ion out flux of $0.5 \times 10^{23} \text{ s}^{-1}$ into the scrape-off-layer, the peak heat load is estimated to be 70 MW/m^2 on the outer target on the initial divertor design (vertical target). This value exceeds significantly the allowable level of 10 MW/m^2 being an initial design target. By installing the “V-shaped corner” in bottom of the outer divertor target, and introducing the deuterium gas puff or argon impurity suitably, the detached condition with high particle recycling and radiation loss conditions is formed, and the peak heat load is successfully reduced below 10 MW/m^2 . It can also be demonstrated properly by reducing the exhaust power at small amount of gas puff flux and argon fraction.

1. Introduction

The compact DEMO reactor named ‘SlimCS’ proposed in Japan Atomic Energy Agency (JAEA) aims to produce the fusion power of $\leq 3 \text{ GW}$ (heating power of 600~700 MW) with a low-aspect-ratio ($A = 2.6$) and a reduced-size center solenoid for economic viability (FIG.1) [1].

This heating power is about 6 times larger than that for ITER [2], but a tolerable heat load on divertor target is restricted below 10 MW/m^2 being an initial design target, which is less by half than that for ITER. Handling of the huge exhaust power in SOL/divertor regions is one of key issues to validate the design parameters of SlimCS. A scenario of power handling is shown that 10~20% of heating power is radiated in the core by argon (Ar) impurity injection and the remaining power of 500~600 MW is exhausted into SOL/divertor region. Whereas, the heat load on divertor target must be kept below 10 MW/m^2 on this huge exhaust power environment. A divertor design is planned to be compatible with it. (1) Vertical target, and deuterium gas puffing and introduction of Ar impurity are used to enhance the particle recycling and the radiation loss power along the divertor leg. (2) Recycling neutrals of ~3% in the divertor

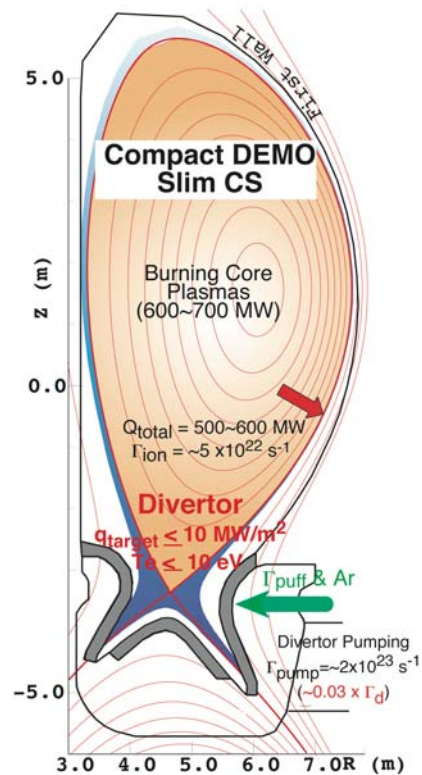


Fig.1. Plasma configuration on the Slim CS DEMO reactor ($R_p=5.5 \text{ m}$, $a_p=2.15 \text{ m}$, $\kappa_{95}=2.0$, $\delta_{95}=0.27$, $q_{95}=4.7$, $I_p=17.5 \text{ MA}$, $B_t=6.0 \text{ T}$, $V_p=924 \text{ m}^3$). The volume averaged density $\langle n_e \rangle \sim 1 \times 10^{20} \text{ m}^{-3}$ and $\tau_p^{\text{core}} \sim 2 \text{ s}$ are assumed. SOL plasma is described in the region of outer midplane width of 3cm. Divertor geometry with the first conceptual (vertical target) design is also included.

are pumped through the inner and outer exhaust slots from the exhaust chamber under the dome to the pumping port. (3) SOL plasma in width of 3 cm at the outer midplane, which is larger than the e-folding length of particle flux profile, is guided into the divertor to take in a large amount of particle flux.

In order to estimate the heat controllability on the conceptual divertor design and to obtain the favorable feature, we carry out the simulation using a divertor code SOLDOR/NEUT2D [3-5] for the first time. This code has been developed in JAEA for the interpretation and prediction of the behaviour of SOL/divertor plasmas in the JT-60 tokamak [6]. Distinctive characteristics of this code are briefly described in section 2. In section 3, the effect of the “*V-shaped corner*” in the bottom of divertor target likely as the ITER and JT-60SA [5,7] is shown to reduce the target heat load with enhancement of the particle recycling and the radiation loss power. Then effects of deuterium gas puffing and introduction of Ar impurity are investigated to obtain the critical low heat load, describing in section 4. In section 5, we show that the heat load is reduced exponentially with decrease of the exhaust power, i.e. the fusion power. Finally, summary is given in section 6.

2. SOLDOR/NEUT2D Code

The SOLDOR/NEUT2D code couples the 2D plasma multi-fluid modeling code SOLDOR with the neutral Monte Carlo (MC) code NEUT2D. Transport of plasma and neutral is solved consistently with their coupled code. Validation has been confirmed by benchmark with the B2.5-EIRENE (SOLPS5.0) code [8] and comparisons of JT-60U experimental results [9]. For the estimation of heat load on the divertor target, the parallel heat flux is evaluated using the expression of $q_{//\text{heat}} = \gamma n_d C_{sd} T_d + n_d C_{sd} E_{ion}$. The explanation for each symbol is found in Ref. [10]. First term of right side in this formula is the contribution from the conductive and convective heat flux of electrons and ions. The heat load associated with release of the ionization energy (13.6 eV) at recombination is contained in the second term. In usual, the contribution from the conductive and convective heat flux of electrons and ions has only been treated as the “*intrinsic heat load*”. At this time, effects of two components are considered and added in this code. The radiation loss power contributes to the heat load on the target in case of the localized radiation profile near the target. We evaluate such heat load with the modified NEUT2D code, where the photons are traced instead of neutral hydrogen particles until they hit the target or the vessel wall. For simplicity, the effect of opaque of plasma is neglected. In addition, the contribution of the neutral particle energy is also included since high recycling condition is expected.

The plasma boundary is set at $r/a = 0.95$ for the simulation. Total exhaust power and ion flux (Q_{total} , Γ_{ion}) across $r/a = 0.95$ are given as input parameters. Particle diffusion coefficient, and thermal electron and ion diffusivity are fixed as $D = 0.3 \text{ m}^2/\text{s}$, and $\chi_{e\perp} = \chi_{i\perp} = 1 \text{ m}^2/\text{s}$ based on the empirical values for various tokamaks. For a treatment of

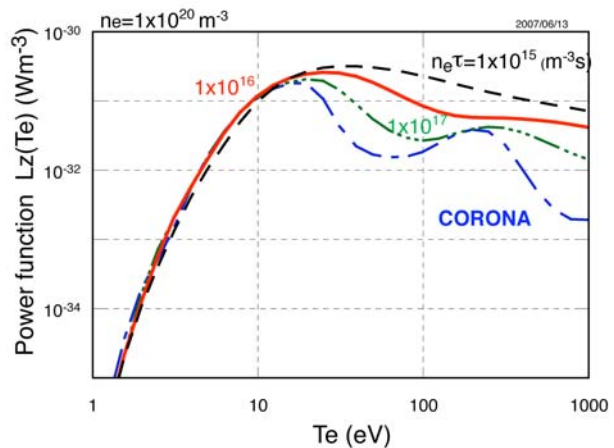


FIG.2. Radiation loss rate coefficients of the argon (Ar) impurity for the simplified non-coronal model.

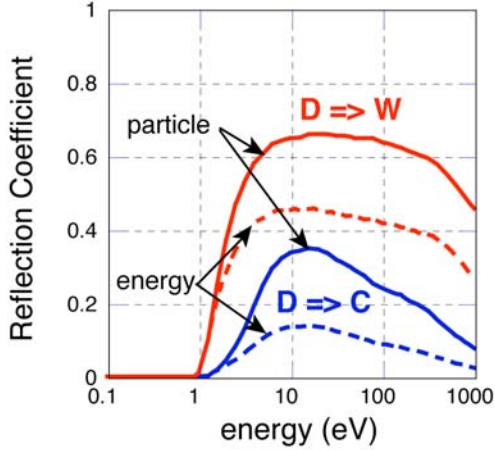


FIG.3. Reflection coefficients of energy and particle of deuterium to the tungsten and carbon materials.

impurity, a simple non-coronal model is employed in the current code. The fraction of Ar impurity to the ion density (n_{Ar}/n_i) is given in the SOL/divertor regions and radiation loss power is evaluated by $W_r = -n_e n_z L_z(T_e)$. Its loss rate $L_z(T_e)$ is used on a residence parameter $n_e \tau_{res} = 1 \times 10^{16} \text{ s/m}^3$ as shown in FIG.2 [11,12]. The recycling of deuterium is assumed to be 100% at the first wall. The first wall material is assumed to be tungsten (W), which the reflection coefficients of particle and energy are almost twice larger than that for carbon as shown in FIG.3. The pumping speed, which is fixed to $S_{pump} = 200 \text{ m}^3/\text{s}$ in this study, is specified by an albed for

neutrals at the entrance of the pumping port.

3. Simulation of divertor performance in the SlimCS

The SOLDOR/NEUT2D code is applied to an initial divertor geometry and a modified geometry with the “V-shaped corner” as shown the mesh structure in FIGs.3(a-1) and (b-1). The $Q_{total} = 500 \text{ MW}$ and $\Gamma_{ion} = 0.5 \times 10^{23} \text{ s}^{-1}$ are used on the basis of the heating power, averaged density and particle confinement time. Gas puff flux of deuterium from outer

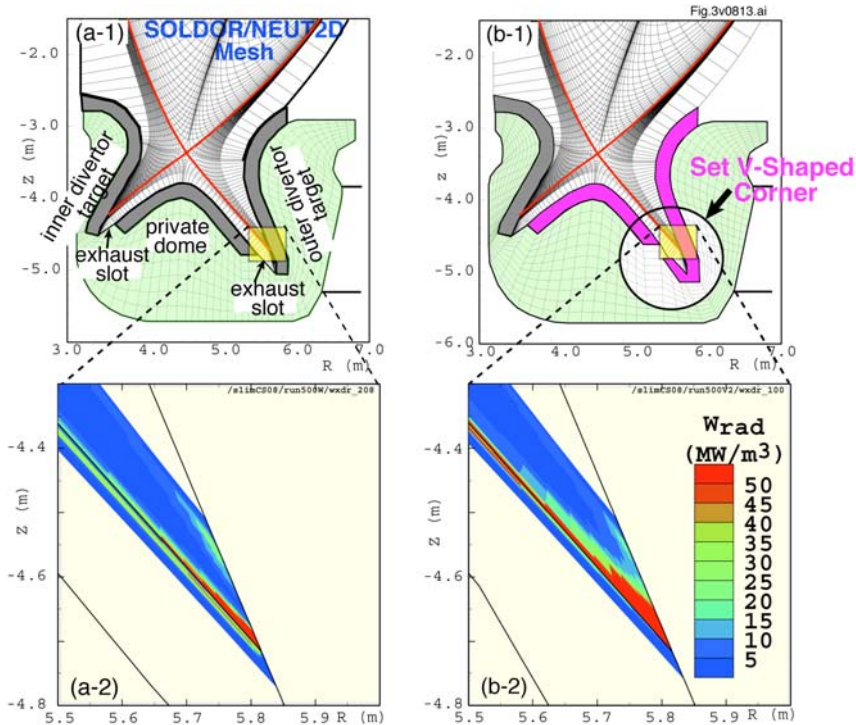


FIG.4. (a-1),(b-1): SlimCS divertor geometry at the initial design and the modified design with installation of the “V-shaped corner”. (a-2),(b-2): Contour plots of radiation loss power density at outer divertor target on both geometry. Input parameters are $Q_{total} = 500 \text{ MW}$, $\Gamma_{ion} = 0.5 \times 10^{23} \text{ s}^{-1}$, $\Gamma_{puff} = 1 \times 10^{23} \text{ s}^{-1}$ and $(n_{Ar}/n_i)_{odp} = 2.0\%$.

divertor wall is given relatively large to $\Gamma_{\text{puff}} = 1 \times 10^{23} \text{ s}^{-1}$. The Ar fraction is assumed to $(n_{\text{Ar}}/n_{\text{i}})_{\text{odp}} = 2\%$ in the outer divertor region and to $(n_{\text{Ar}}/n_{\text{i}})_{\text{other}} = 1\%$ in other parts. The SOL electron density at the middle of outer separatrix corresponds to $\sim 3.3 \times 10^{19} \text{ m}^{-3}$.

For the first conceptual divertor design as shown in FIG.4(a-1), a completely detached condition takes place on inner divertor target with the target heat load below 5 MW/m^2 . On the other hand, a detached condition on the outer divertor target is partially formed just under the separatrix strike point as shown in FIG.5(a-1). Significantly high temperature of electron and ion is held at outside of separatrix on the target with their peak temperature of $T_{\text{e-peak}} = 49 \text{ eV}$ and $T_{\text{i-peak}} = 194 \text{ eV}$, respectively. Those conditions produce a severe heat load on the outer target as shown in FIG.5 (a-2). The peak heat load by the total loss power from the contributions of electron/ion conduction and convection (“intrinsic heat load”), recombination, radiation, and neutrals reaches to $\sim 70 \text{ MW/m}^2$, which is seriously exceeding 10 MW/m^2 .

To build up to the high recycling and radiation loss conditions in outer divertor and to reduce the heat load, the “V-shaped corner” likely as the ITER and JT-60SA is installed in the bottom of outer divertor target (FIG.4(b-1)). Typical results are obtained that the radiation loss power

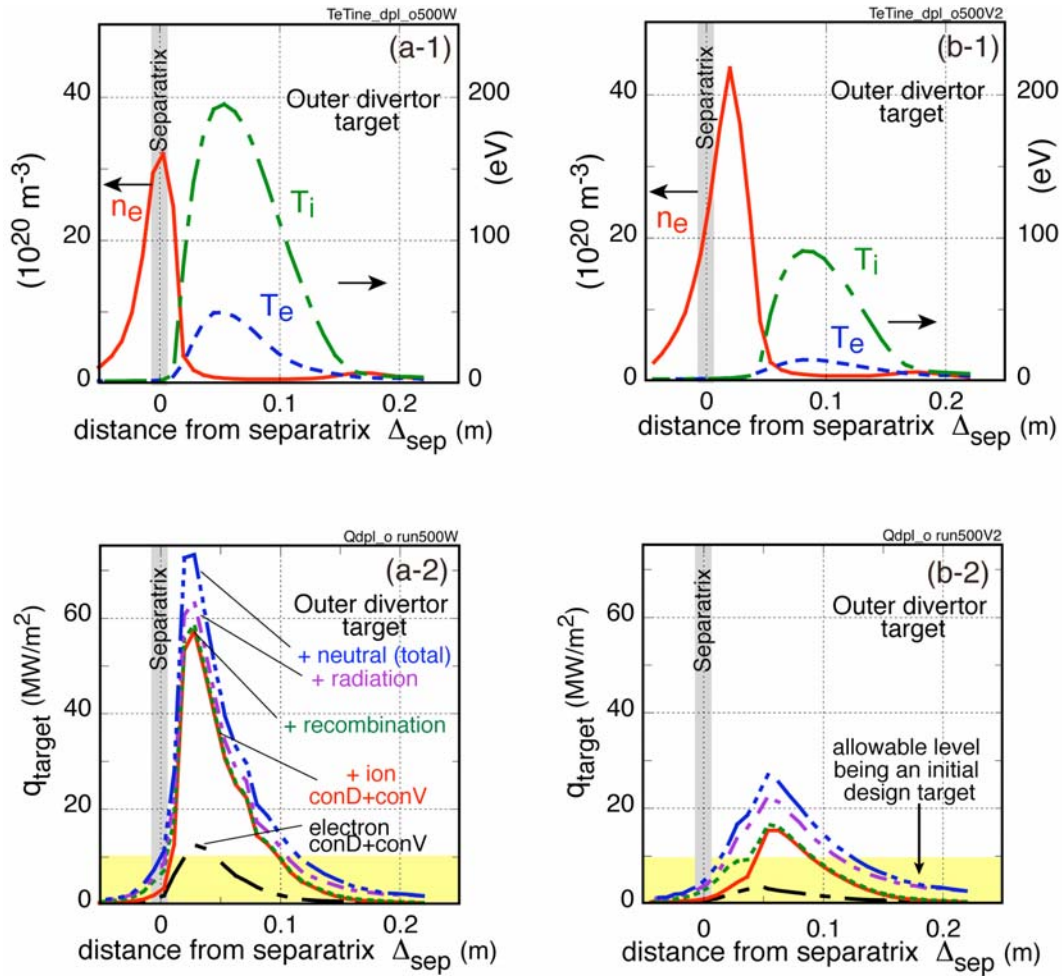


FIG.5. Profiles of electron density n_{e} , electron temperature T_{e} and ion temperature T_{i} on the outer divertor target at the geometry of the initial design (a-1) and the modified design with the “V-shaped corner” (b-1). (a-2), (b-2) Those for heat load q_{target} profiles, where the total heat load consists of the contributions of electron/ion conduction and convection (intrinsic heat load), recombination, radiation and neutral power losses.

is increased from 85 MW to 142 MW in outer divertor region and the neutral flux is also increased from $3.7 \times 10^{24} \text{ s}^{-1}$ to $4.2 \times 10^{24} \text{ s}^{-1}$ by enhancement of recycling. 2D profiles of radiation loss power density on both geometry (FIGs.4(a-2), (b-2)) show that the power concentrates around the separatrix strike point at the V-shaped geometry. They bring higher density and lower temperature than those at the initial geometry, and expansion of the detached regions as shown in FIG.5(b-1). Consequently, the peak heat load can be reduced predicatively by 27 MW/m^2 as shown in FIG.5(b-2). Although a ratio of the heat load from recombination, radiation, and neutral loss power to the total heat load is increased from 22% at the initial design to 43% at the V-shaped geometry with those enhancements, drop of the intrinsic heat load from electron/ion conduction and convection loss power is remarkable.

Whereas, the total heat load is still over the heat load level of initial design target even in this condition. To obtain a critical low heat load, we examine to increase the gas puff flux and Ar fraction in simulations, and their dependences are studied in next section.

4. Effects of gas puffing and introduction of Ar impurity

Further reduction of the heat load is still needed even if the “V-shaped corner” is installed in the bottom of outer divertor target as mentioned above. In order to attain it, we simulate the effect of increment of the divertor gas puffing and introduction of Ar impurity to enhance the remote radiation cooling.

At first, to estimate an effect of deuterium gas puffing to the divertor plasma condition and to obtain the heat load below 10 MW/m^2 , the gas puff flux is changed in the regions of $\Gamma_{\text{puff}} = 0.5 \sim 2.0 \times 10^{23} \text{ s}^{-1}$ with the V-shaped divertor geometry. Other parameters are fixed as $Q_{\text{total}} = 500 \text{ MW}$, $\Gamma_{\text{ion}} = 0.5 \times 10^{23} \text{ s}^{-1}$, $(n_{\text{Ar}}/n_{\text{i}})_{\text{odp}} = 2\%$, $(n_{\text{Ar}}/n_{\text{i}})_{\text{other}} = 1\%$, $S_{\text{pump}} = 200 \text{ m}^3/\text{s}$. FIG.6 shows the dependences of gas puff flux on the target peak heat load $q_{\text{target}}^{\text{peak}}$, radiation loss power in outer divertor region, peak electron temperature and that for separatrix strike point on the outer divertor target, and divertor pumping rate (pumping flux / recycling neutrals in the divertor regions).

Results show that the target

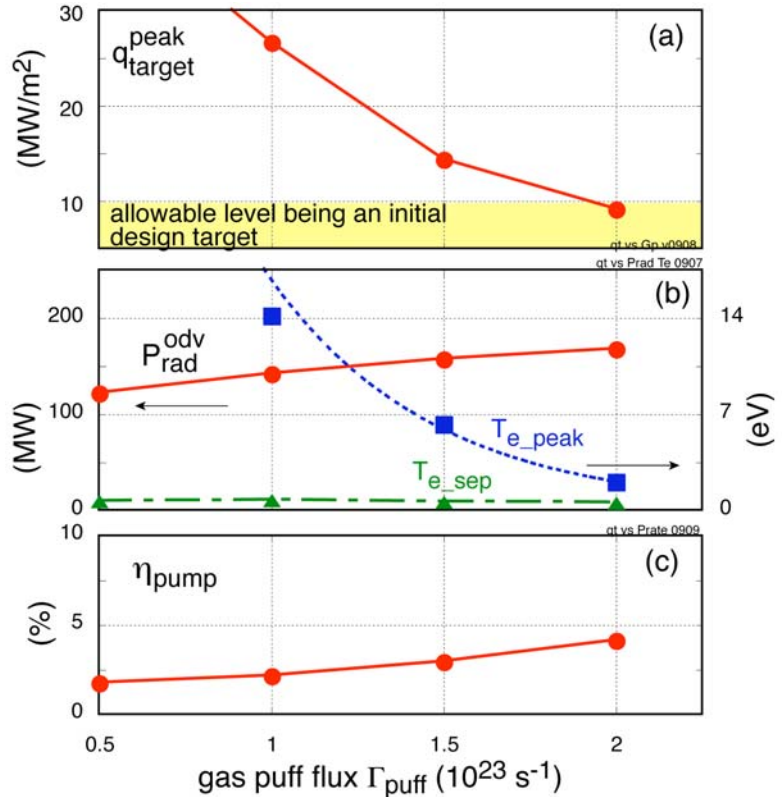


FIG. 6. Dependences of the gas puff flux Γ_{puff} on (a) peak heat load at the outer target $q_{\text{target}}^{\text{peak}}$, (b) radiation loss power in the outer divertor region $P_{\text{rad}}^{\text{odv}}$, electron temperature at the separatrix strike point $T_{\text{e_sep}}$ and the peak value at outside of strike point on the target $T_{\text{e_peak}}$, and (c) divertor pumping rate (pumping flux / recycling neutrals) η_{pump} . Other parameters are same as a case of FIG.5(b).

heat load decreases with increase of the gas puff flux as shown in FIG.6(a) and then it reaches to 9 MW/m^2 at $\Gamma_{\text{puff}} = 2 \times 10^{23} \text{ s}^{-1}$, which comes into 10 MW/m^2 . Radiation loss power is increased gradually from 120 MW to 160 MW with the gas puff flux. The electron temperature at the separatrix strike point on the target is almost constant ($< 1 \text{ eV}$) with sustaining the detachment in this region. Besides, the peak temperature on outside of the strike point is decreased exponentially with accompanying the change of plasma condition. Partial detachment condition at low gas puff case progresses to be completely with increase of the gas puff flux. Exponential reduction of the electron temperature is important to reduce the erosion by the physical sputtering which is enhanced as a strong positive function of the temperature [12]. The pumping rate along the divertor conception ($\sim 3\%$) can be obtained on above conditions as shown in FIG.6(c). It is increased from 2% to 4% by increase the neutral density in the exhaust chamber with progress of the detachment. In this way, a property of the gas puffing is shown for reduction of the heat load and temperature on the target.

Secondly, the effect of a noble gas Ar with medium Z ($= 18$) is investigated for radiation cooling since it has a high radiation loss rate [12]. The Ar fraction is changed from $(n_{\text{Ar}}/n_{\text{i}})_{\text{odp}} = 1.5\%$ to 5% in the outer divertor region. Other parameters are fixed as $Q_{\text{total}} = 500 \text{ MW}$, $\Gamma_{\text{ion}} = 0.5 \times 10^{23} \text{ s}^{-1}$, $\Gamma_{\text{puff}} = 1 \times 10^{23} \text{ s}^{-1}$, $(n_{\text{Ar}}/n_{\text{i}})_{\text{other}} = 1\%$, $S_{\text{pump}} = 200 \text{ m}^3/\text{s}$. FIG.7 shows the dependences of Ar fraction on the target peak heat load, radiation loss power, peak electron temperature and that for separatrix strike point, and pumping rate. The heat load of 47 MW/m^2 at $(n_{\text{Ar}}/n_{\text{i}})_{\text{odp}} = 1.5\%$ is decreased with increase of the Ar fraction as shown in FIG.7(a). Then it is also reduced by 9 MW/m^2 at the $(n_{\text{Ar}}/n_{\text{i}})_{\text{odp}} = 5\%$, coming into the allowable level.

Radiation loss power is enhanced to 210 MW at this case, which becomes larger $\sim 20\%$ than that for the gas puffing case at the heat load of 9 MW/m^2 . Condition of detachment under the separatrix strike point is kept with the electron temperature below 1 eV as shown in FIG.7(b) similar as the gas puffing case. While, drop of peak electron temperature at outside of the separatrix strike point by increase of the Ar fraction is declined as the heat reduction developed. As a result, the plasma detachment condition is still partially even at the critical case of $q_{\text{target}}^{\text{peak}} = 9 \text{ MW/m}^2$ and change of the pumping rate stays in $2\% \sim 3\%$ with a gradual increase of neutral density in the exhaust chamber. Thus, a role of the introduction of Ar impurity

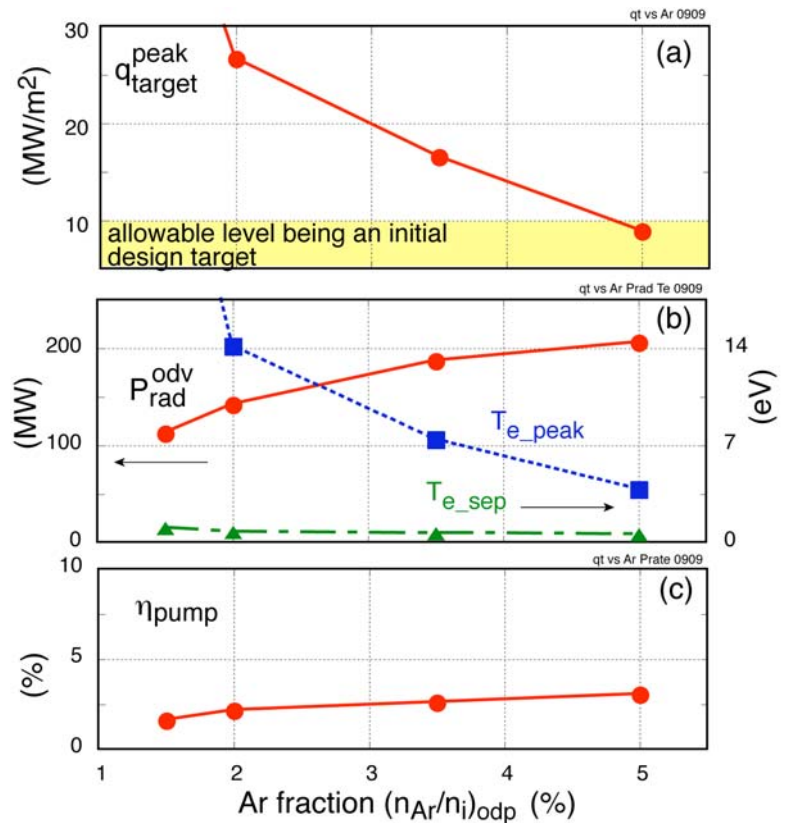


FIG. 7. Dependences of the Ar fraction $(n_{\text{Ar}}/n_{\text{i}})_{\text{odp}}$ in outer divertor region on (a) $q_{\text{target}}^{\text{peak}}$, (b) $P_{\text{rad}}^{\text{odv}}$, $T_{\text{e_sep}}$ and $T_{\text{e_peak}}$, and (c) η_{pump} . Other parameters are same as a case of FIG.5(b).

for reduction of the heat load is characterized similar as that for the gas puffing.

These indicate generally that relatively large amount of gas puff flux or Ar fraction is necessary to obtain a critical low heat load. Although the compatibility of the high core confinement with the radiative cooling divertor by the strong gas puffing or introduction of Ar impurity can not be predicted using only the divertor code (which will be evaluated elsewhere), it is apprehensive for an influence of the core plasma capability. As another way, to lower the exhaust power with decrease of the fusion output is a direct method to reduce the heat load with small amount of gas puff flux or Ar fraction. Its simulation is shown as below.

5. Dependence of the heat load on the exhaust power

A dependence of the exhausted power on the heat load is evaluated by decreasing the exhaust power from $Q_{\text{total}} = 600$ MW to 300 MW at constant gas puff flux of $\Gamma_{\text{puff}} = 1 \times 10^{23} \text{ s}^{-1}$, and Ar fraction of $(n_{\text{Ar}}/n_{\text{i}})_{\text{odp}} = 2\%$. The exhaust ion flux and pumping speed are also fixed as $\Gamma_{\text{ion}} = 0.5 \times 10^{23} \text{ s}^{-1}$ and $S_{\text{pump}} = 200 \text{ m}^3/\text{s}$. FIG.8 shows a function of the exhaust power to the peak value of the total heat load as treated before and a component of the intrinsic heat load by the electron/ion conductive and convective power losses. That of total heat load is exponentially reduced from 46 MW/m^2 to 7 MW/m^2 with decrease of the exhaust power. It shows that the heat load below 10 MW/m^2 can be obtained at $Q_{\text{total}} = 300$ MW with a completely detachment condition by smaller amount of gas puff flux and Ar fraction in comparison with the critical case at 500 MW as mentioned in section 4.

While, a ratio of the intrinsic heat load to the total heat load decreases with decrease of Q_{total} . In contrast, it means that the contribution of remaining power losses by recombination, radiation and neutrals is enhanced at the condition for the constant gas puff flux and Ar fraction. Considering an influence to the core plasmas, it is indicated that those ratio to the total heat load is reduced by decreasing the gas puff flux or Ar fraction with compensation of enlargement of the intrinsic heat load at the 300 MW case.

5. Summary

In order to estimate the heat controllability in the divertor and to obtain the favorable feature on the compact DEMO reactor ‘‘SlimCS’’, we carry out the simulation using the SOLDOR/NEUT2D divertor code.

As the SlimCS SOL/divertor parameters are typically set to $Q_{\text{total}} = 500$ MW, $\Gamma_{\text{ion}} = 0.5 \times 10^{23} \text{ s}^{-1}$, $\Gamma_{\text{puff}} = 1 \times 10^{23} \text{ s}^{-1}$, $(n_{\text{Ar}}/n_{\text{i}})_{\text{odp}} = 2\%$ and $S_{\text{pump}} = 200 \text{ m}^3/\text{s}$, the peak heat load reaches to 70 MW/m^2 on the outer divertor target at the initial divertor design, which exceeds seriously over the allowable level of 10 MW/m^2 being an initial design target. By installing the ‘‘V-shaped

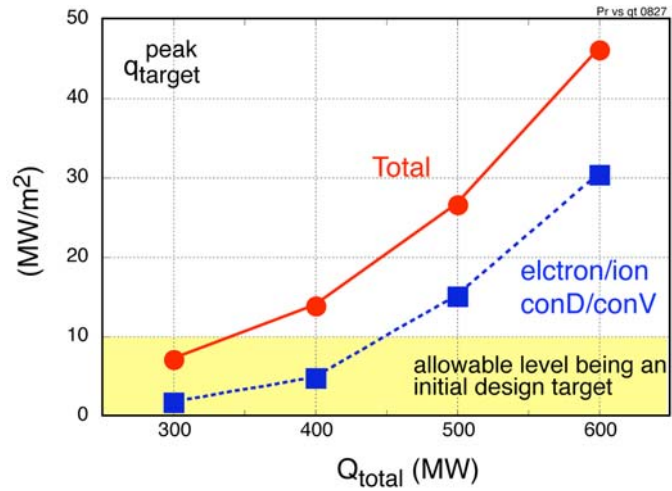


FIG. 8. Dependences of the exhaust power Q_{total} on the total heat load and component of that from electron/ion conduction / convection power losses. Fixed parameters are $\Gamma_{\text{ion}} = 0.5 \times 10^{23} \text{ s}^{-1}$, $\Gamma_{\text{puff}} = 1 \times 10^{23} \text{ s}^{-1}$, $(n_{\text{Ar}}/n_{\text{i}})_{\text{odp}} = 2\%$ and $S_{\text{pump}} = 200 \text{ m}^3/\text{s}$.

corner” in the bottom of the outer target, the peak heat load can be reduced to 27 MW/m^2 with formations of the high recycling and high radiation conditions. In here, drop of the intrinsic heat load from electron/ion conduction and convection loss power is remarkable, but it is noted that contributions from recombination, radiation, and neutral loss power increase with those enhancements. To obtain a critical low heat load below 10 MW/m^2 that is still not achieved in above condition on the V-shaped geometry, the amount of gas puff flux or Ar fraction is changed and characterized as a function of heat load. It can be demonstrated that the heat load is reduced to 9 MW/m^2 with a completely detached condition by increasing the gas puff flux to $\Gamma_{\text{puff}} = 2 \times 10^{23} \text{ s}^{-1}$. That low heat load is also obtained at the Ar fraction of $(n_{Ar}/n_i)_{\text{odp}} = 5\%$ with enhancement of radiation loss power larger than that for the gas puffing case. On the other hand, to lower the exhaust power with decrease of the fusion output is a direct method to reduce the heat load with small amount of gas puff flux or Ar fraction. As expected, the heat load below 10 MW/m^2 can be obtained at $Q_{\text{total}} = 300 \text{ MW}$ with a completely detachment condition at smaller amount of gas puff flux and Ar fraction in comparison with the critical case at 500 MW . The pumping rate is performed $\sim 3\%$ along the divertor conception by $S_{\text{pump}} = 200 \text{ m}^3/\text{s}$ in these studies.

The SOLDOR/NEUT2D simulations show the dependences of the heat load on the divertor geometry, gas puff flux, Ar fraction and exhaust power, and region into the heat load below 10 MW/m^2 in their parameters, which will lead a directionality for further reduction of the heat load even if the allowable heat load level becomes smaller due to the technical requirement [13]. Namely, we obtain a prospect of power handling in the divertor to validate the design parameters of SlimCS through these studies.

Acknowledgements

The authors would like to thank the members of the division of fusion energy technology of JAEA for their fruitful discussions. They are also grateful to the members of the JT-60 team as well as the analysis group for their supports and encouragements. This work is partly supported by JSPS, Grant-in-Aid for Scientific Research (T) No. 19055005.

References

- [1] TOBITA, K., et al., Nucl. Fusion **47** (2007) 892.
- [2] ITER Physics Basis, Nucl. Fusion **47** (2007) S203.
- [3] KAWASHIMA, H., Plasma Phys. Control. Fusion **49** (2007) S77.
- [4] SHIMIZU, K., et al., Contrib. Plasma Phys. **48** (2008) 270.
- [5] KAWASHIMA, H., et al., to be published in Fusion Eng. Design (2008).
- [6] TAKENAGA, H. and the JT-60 Team, Nucl. Fusion **47** (2007) S563.
- [7] KIKUCHI, M., JA-EU satellite tokamak working group and JT-60SA design team, in Proceedings of the 21st IAEA Fusion Energy Conference, Chengdu, China, 2006, (IAEA-CN-149/FT/2-5).
- [8] COSTER, D.P., et al., in Proc of 19th IAEA Fusion Energy Conference (Lyon, France, 2002), IAEA-CN-94/THP2-13.
- [9] KAWASHIMA, H., et al., J. Nucl. Mater. **363-365** (2007) 786.
- [10] KAWASHIMA, H., et al., Plasma Fusion Res. **1** (2006) 031.
- [11] POST, D.E., J. Nucl. Mater. **220-222** (1995) 143.
- [12] ITER Physics Basis, Nucl. Fusion **39** (1999) 2391.
- [13] TOBITA, K., et al., in this conference FT/P3-9.